Structure and magnetic behaviour of the first singly bridged nickel cyanate chain and a new dinuclear complex: an approximation to the superexchange mechanism for the nickel pseudohalide system †

Albert Escuer,*,ᵃ Ramon Vicente,ᵃ M. Salah El Fallah,ᵃ Xavier Solans ᵇ and Mercé Font-Bardía ᵇ

ᵃ *Departament de Química Inorgànica, Universitat de Barcelona, Diagonal 647, 08028-Barcelona, Spain*

ᵇ *Departament de Cristallografia i Mineralogia, Universitat de Barcelona, Martí Franqués s/n, 08028-Barcelona, Spain*

Two new nickel(II) bridging-cyanate complexes of formula [{Ni(323-tet)(μ-OCN)}$_n$][ClO$_4$]$_n$ 1 [323-tet = N,N'-bis(3-aminopropyl)ethane-1,2-diamine] and [{Ni(Me$_6$[14]aneN$_4$)}$_2$(μ-OCN)$_2$][ClO$_4$]$_2$ 2 (Me$_6$[14]aneN$_4$ = DL-5,5,7,12,12,14-hexamethyl-1,4,8,11-tetraazacyclotetradecane) have been synthesized and characterized. The crystal structures of 1 and 2 have been solved and in both compounds the cyanate ligand acts as an end-to-end bridge with the nickel atoms in a NiN$_5$O octahedral environment. Compound 1 is a chain in which the Ni(323-tet) fragments are linked by single cyanate bridges in a *trans* position, whereas compound 2 consists of dinuclear units with two cyanate bridges in a *cis* arrangement. Magnetic measurements in the 2–300 K range indicate weak ferromagnetism for 1 and antiferromagnetic behaviour for 2. Magneto-structural correlations have been obtained by Extended-Hückel calculations and a generic superexchange model for the nickel(II) pseudohalogen system is proposed.

Considerable attention has been devoted in recent years to the study, from synthetic and magnetic points of view, of polynuclear complexes of nickel(II) in which pseudohalogen bridges act as a superexchange pathway. The nickel azido system is the most widely studied and, from experimental data, the most characteristic feature of the azido bridges is the relationship between co-ordination mode and magnetic behaviour: end-to-end co-ordination is associated with antiferromagnetic behaviour and end-on co-ordination with ferromagnetic behaviour. For the end-to-end co-ordination mode, a large number of azido compounds with different nuclearities from dimers[1–5] to one-dimensional chains[6–11] have been characterized. Models to correlate the magnitude of the coupling with the structure of the complexes with end-to-end azido bridges have been successfully proposed.[4,10] In contrast, the polynuclear chemistry of nickel(II) cyanate systems is scarce and only two dinuclear compounds have been structurally characterized: the first by Duggan and Hendrickson in 1973, with formula [{Ni(tren)}$_2$(μ-OCN)$_2$][BPh$_4$]$_2$ [tren = tris(2-aminoethyl)amine], shows the cyanate co-ordinated in the end-to-end mode and is weakly antiferromagnetic.[12–14] The second compound, with formula [{Ni(terpy)(H$_2$O)}$_2$-(μ-OCN)$_2$][PF$_6$]$_2$ (terpy = 2,2′:6′,2″-terpyridine), has two end-on N-cyanate bridges and shows weak ferromagnetic behaviour.[15,16]

In order to obtain new structural and magnetic data on the nickel(II) cyanate system we have attempted to obtain new polynuclear complexes by the same strategy as that applied successfully with the azido ligand,[7–10] which consists of the reaction of cyanate with [NiL]$^{2+}$ units (L = open or macrocyclic tetraaminated ligands), for which the *trans* co-ordination is preferred, in order to obtain *trans*-monobridged one-dimensional systems. The synthesis failed when L was a macrocyclic ligand such as 1,4,8,11-tetraazacyclotetradecane (cyclam) or methylated derivatives such as *meso*-5,5,7,12,12,14-hexamethyl- or 1,4,8,11-tetramethyl-1,4,8,11-tetraazacyclo-

tetradecane, for which only mononuclear complexes were obtained.[17] However, starting from open tetraaminated ligands such as N,N'-bis(3-aminopropyl)ethane-1,2-diamine (323-tet), the one-dimensional compound [{Ni(323-tet)(μ-OCN)}$_n$]-[ClO$_4$]$_n$ 1 was characterized. Some structural and magnetic features of 1 have previously been advanced in a preliminary communication.[18] Starting from the macrocycle DL-5,5,7,12,12,14-hexamethyl-1,4,8,11-tetraazacyclotetradecane (Me$_6$[14]aneN$_4$), for which the *cis* co-ordination is preferred, a new dinuclear complex with a double cyanate bridge, [{Ni(Me$_6$[14]aneN$_4$)}$_2$(μ-OCN)$_2$][ClO$_4$]$_2$ 2, was also characterized. The cyanate ligand is end-to-end co-ordinated in the two compounds, but 1 is ferromagnetic whereas 2 shows antiferromagnetic behaviour.

The aim of this paper is to study the co-ordination and magnetic properties of the end-to-end cyanate bridges and summarize the general trends of the superexchange through the azido, cyanate, thio- and seleno-cyanate pseudohalogen bridges. This study also describes the first cyanate-bridged one-dimensional compound synthesized to date for a paramagnetic centre other than copper(II), for which the cyanate bridge is poorly relevant magnetically due to the large Cu–O bond distance.[19,20]

Experimental

Synthesis

CAUTION! Perchlorate salts of metal complexes with organic ligands are potentially explosive. Only a small amount of material should be prepared and it should be handled with caution.

[{Ni(323-tet)(μ-OCN)}$_n$][ClO$_4$]$_n$ 1 was synthesized as previously described.[18]

[{Ni(Me$_6$[14]aneN$_4$)}$_2$(μ-OCN)$_2$][ClO$_4$]$_2$ 2

To a stirred hot suspension of [Ni(Me$_6$[14]aneN$_4$)][ClO$_4$]$_2$[21] (2 g, 3.7 mmol) in water (50 cm³), NaOCN (1.20 g, 18 mmol) in water (10 cm³) was added. Immediately a green precipitate was

Table 1 Crystal data for [{Ni(323-tet)(μ-OCN)}$_n$][ClO$_4$]$_n$ 1 and [{Ni(Me$_6$[14]aneN$_4$)}$_2$(μ-OCN)$_2$][ClO$_4$]$_2$ 2

Formula	C$_{9n}$H$_{22n}$N$_{5n}$Ni$_n$O$_n$·nClO$_4$	C$_{34}$H$_{72}$N$_{10}$Ni$_2$O$_2$·2ClO$_4$
M	374.47	969.34
Crystal system	Monoclinic	Orthorhombic
Space group	$P2_1/n$	$Pbca$
a/Å	10.587(2)	14.879(5)
b/Å	12.395(2)	15.385(4)
c/Å	11.871(2)	19.990(4)
β/°	92.00(1)	90
U/Å^3	1556.8(8)	4576(2)
Z	4	4
D_c/g cm^{-3}	1.597	1.407
μ(Mo-Kα)/cm^{-1}	14.44	10.01
$F(000)$	784.0	2064
T/°C	25	25
No. of parameters refined	281	300
R^a	0.038	0.047
R_w/$wR^{2\,b}$	0.041	0.115

^{a} $R(F_o) = \Sigma||F_o| - |F_c||/\Sigma|F_o|$. ^{b} $R_w(F_o) = \Sigma||F_o| - |F_c||/\Sigma w|F_o|$ for 1 and $wR^2 = \{\Sigma[(F_o)^2 - (F_c)^2]^2/\Sigma(F_o)^4\}^{\frac{1}{2}}$.

formed. After 30 min of vigorous stirring the compound was filtered and washed with small quantities of water and acetone. Recrystallization from acetonitrile gave green crystals suitable for an X-ray crystal-structure determination (Found: C, 42.1; H, 7.4; N, 14.3; Cl, 7.1. Calc. for C$_{34}$H$_{72}$Cl$_2$N$_{10}$Ni$_2$O$_{10}$: C, 42.10; H, 7.50; N, 14.45; Cl, 7.30%).

Spectral and magnetic measurements

IR spectra were recorded on a Nicolet 520 FTIR spectrophotometer. Magnetic measurements were carried out on polycrystalline samples with a SQUID apparatus working in the range 2–300 K for 1 under a field of 0.3 T and a pendulum-type magnetometer (Manics DSM8) equipped with a helium continuous-flow cryostat working in the 4–300 K range for 2 under a magnetic field of approximately 1.5 T. Diamagnetic corrections were estimated from Pascal Tables.

Crystal data collection and refinement

Crystals (0.1 × 0.1 × 0.2 mm) of 1 and 2 were selected and mounted on an Enraf-Nonius CAD4 diffractometer. The crystallographic data, conditions retained for the intensity data collection and some features of the structure refinement are listed in Table 1. Accurate unit-cell parameters were determined from automatic centring of 25 reflections (16 < θ < 21° for 1 and 12 < θ < 21° for 2) and refined by the least-squares method. Intensities were collected with graphite-monochromatized Mo-Kα radiation (λ = 0.710 69 Å), using the ω–2θ scan technique.

A total of 4952 (1) and 6631 (2) reflections were measured in the 2 < θ < 30° range; 4033 (1) and 3149 (2) reflections were assumed to be observed applying the condition I > 2.5$\sigma(I)$. Three reflections were measured every 2 h as orientation and intensity control; significant intensity decay was not observed. Corrections were made for Lorentz polarization but not for absorption. The structure was solved by Patterson synthesis using the SHELXS computer program[22] and refined by full-matrix least squares, using the SHELX 76[23] (1) and SHELXL 93[24] (2) computer programs. The function minimized was $\Sigma w(|F_o| - |F_c|)^2$, where $w = [\sigma^2(F_o) + 0.0003|F_o|^2]^{-1}$ for 1 and $\Sigma w(|F_o|^2 - |F_c|^2)^2$, where $w = [\sigma^2(I) + (0.0806P)^2 + 2.0959P]^{-1}$ and $P = (|F_o|^2 + 2|F_c|^2)/3$ for 2, f, f' and f'' were taken from ref. 25. For 1, three oxygen atoms of the perchlorate ion were disordered, and an occupancy factor of 0.5 was assigned according to the height of the Fourier synthesis. The position of the H atoms was located from a difference synthesis and refined with an overall isotropic thermal parameter, while the remaining atoms were refined anisotropically. For 2 all H atoms were computed and refined with an overall isotropic

thermal parameter using a riding model. The final R factor was 0.038 (R' = 0.041) for 1 and R (on F) = 0.047 [R' (on $|F|^2$) = 0.115], goodness-of-fit 0.965 for all observed reflections for 2. The number of refined parameters was 281 (1) and 300 (2) respectively. Maximum shift/e.s.d. = 0.1 and 0.3 and maximum and minimum peaks in the final difference synthesis were 0.3, −0.3 and 0.397, −0.401 e Å^{-3} for 1 and 2 respectively.

Final atomic coordinates for compounds 1 and 2 are given in Tables 2 and 3 respectively.

Complete atomic coordinates, thermal parameters and bond lengths and angles have been deposited at the Cambridge Crystallographic Data Centre. See Instructions for Authors, *J. Chem. Soc., Dalton Trans.*, 1996, Issue 1.

Results and Discussion

IR spectra

The characteristic bands attributable to the aminate ligands appear at ν(N–H) 3326, 3277, 2944, 2874, 1595, 1471 and 1436 cm^{-1} for 1 and 3225, 2975, 2925, 1310, 1270 and 1230 cm^{-1} for 2. The ν_{asym}(CO) appears at 2200 (1) and 2235 cm^{-1} (2) as a strong symmetrical absorption. The two compounds show similar bands at 1100 and 600 cm^{-1} due to the perchlorate anions.

Description of the structures

[{Ni(323-tet)(μ-OCN)}$_n$][ClO$_4$]$_n$ 1. The structure consists of parallel one-dimensional nickel cyanate chains in a *trans* arrangement, isolated by ClO$_4^-$ counter anions found in the interchain space. An atom-labelling scheme and a view of the unit cell are shown in Fig. 1. The main bond distances and angles are gathered in Table 4. The four Ni–N distances are similar [2.105(2), 2.098(2), 2.099(2) and 2.072(2) Å] and the four atoms of the 323-tet ligand and the nickel atom are in the same plane [maximum deviation from the mean plane 0.09 Å in N(4)]. The co-ordination of the cyanate bridge shows strongly asymmetric bond lengths and angles: Ni–O(1) 2.258(1), Ni–N(1) 2.068(2) Å, Ni–O(1)–C(1) 132.0(1) and Ni–N(1)–C(1^I) 163.3(1)°. The Ni–OCN–Ni torsion angle is 22.6° and as a consequence of both factors (asymmetric Ni–X–C bond angles and the Ni–NCO–Ni torsion angle), the angle between the normals to the two neighbouring NiN$_4$ 323-tet planes is 27.8°; Ni$\cdots$Ni intrachain distance is 6.284(1) Å.

[{Ni(Me$_6$[14]aneN$_4$)}$_2$(μ-OCN)$_2$][ClO$_4$]$_2$ 2. The unit cell contains four centrosymmetric [Ni$_2$(Me$_6$[14]aneN$_4$)$_2$(OCN)$_2$]$^{2+}$ dinuclear entities isolated by eight perchlorate counter anions.

Table 2 Atomic coordinates for compound **1** with estimated standard deviations (e.s.d.s) in parentheses

Atom	X/a	Y/b	Z/c	Atom	X/a	Y/b	Z/c
Ni	0.237 47(2)	0.133 67(2)	0.207 25(2)	C(6)	0.227 9(3)	0.210 7(2)	−0.022 9(2)
Cl	−0.169 50(5)	−0.111 56(4)	0.386 03(5)	C(7)	0.010 9(2)	0.190 2(2)	0.043 3(2)
N(1)	0.233 2(2)	0.294 8(1)	0.251 9(2)	C(8)	−0.071 8(3)	0.131 6(2)	0.123 1(3)
N(2)	0.350 5(2)	0.093 5(2)	0.350 6(2)	C(9)	−0.043 8(2)	0.157 4(2)	0.246 5(2)
N(3)	0.397 2(2)	0.162 7(1)	0.112 0(1)	O(1)	0.241 5(2)	−0.039 5(1)	0.148 6(1)
N(4)	0.142 9(2)	0.151 7(1)	0.050 0(1)	O(2)	−0.072 6(11)	−0.108 5(7)	0.308 2(9)
N(5)	0.072 2(2)	0.103 7(2)	0.290 4(2)	O(3)	−0.183 6(2)	−0.009 4(2)	0.439 9(2)
C(1)	0.254 1(2)	−0.124 4(1)	0.199 7(2)	O(4)	−0.174 8(9)	−0.197 8(6)	0.466 0(7)
C(2)	0.476 2(2)	0.044 1(2)	0.339 1(2)	O(5)	−0.268 0(10)	−0.129 8(7)	0.305 6(6)
C(3)	0.555 7(2)	0.103 3(2)	0.256 0(2)	O(2')	0.552 8(7)	0.380 8(6)	0.166 6(10)
C(4)	0.508 6(2)	0.094 3(2)	0.134 3(2)	O(4')	0.149 7(13)	0.192 7(9)	0.530 1(10)
C(5)	0.358 1(3)	0.161 3(3)	−0.007 7(2)	O(5')	0.283 0(9)	0.135 0(10)	0.670 8(13)

Table 3 Atomic coordinates for compound **2** with e.s.d.s in parentheses

Atom	X/a	Y/b	Z/c	Atom	X/a	Y/b	Z/c
Ni	0.1244(1)	0.1116(1)	0.0514(1)	C(10)	0.3055(2)	0.0748(3)	−0.0119(2)
Cl	0.3851(1)	0.2779(1)	0.1481(1)	C(11)	−0.0256(3)	0.0627(3)	0.1920(2)
O	−0.0214(2)	0.1256(2)	0.0327(2)	C(12)	0.0974(4)	0.0388(3)	0.2721(2)
N(1)	0.1112(2)	−0.0108(2)	0.0088(2)	C(13)	0.0550(4)	0.3346(3)	0.1867(3)
N(2)	0.2638(2)	0.0922(2)	0.0544(2)	C(14)	0.1758(3)	0.0955(4)	−0.1312(2)
N(3)	0.1260(2)	0.0487(2)	0.1487(2)	C(15)	0.2232(3)	0.2494(4)	−0.1386(2)
N(4)	0.1140(2)	0.2335(2)	0.0991(2)	C(16)	0.4038(3)	0.0483(3)	−0.0056(3)
N(5)	0.1395(2)	0.1922(2)	−0.0384(1)	C(17)	−0.0662(2)	0.0667(2)	0.0107(2)
C(1)	0.2760(3)	0.0208(3)	0.1025(2)	O(1)	0.4537(7)	0.3338(10)	0.1401(8)
C(2)	0.2230(3)	0.0387(3)	0.1641(2)	O(2)	0.3210(15)	0.2868(15)	0.0962(10)
C(3)	0.0714(3)	0.0828(3)	0.2060(2)	O(3)	0.3485(17)	0.2997(20)	0.2112(11)
C(4)	0.0868(3)	0.1811(3)	0.2143(2)	O(4)	0.4080(17)	0.1966(8)	0.1544(15)
C(5)	0.0563(3)	0.2412(3)	0.1596(2)	O(1')	0.4348(12)	0.3503(7)	0.1585(10)
C(6)	0.0860(3)	0.2937(2)	0.0459(2)	O(2')	0.3095(14)	0.2971(19)	0.1147(13)
C(7)	0.1443(3)	0.2819(2)	−0.0141(2)	O(3')	0.3629(14)	0.2340(14)	0.2014(9)
C(8)	0.2098(3)	0.1720(3)	−0.0904(2)	O(4')	0.4478(12)	0.2215(13)	0.1154(10)
C(9)	0.2993(3)	0.1540(3)	−0.0571(2)				
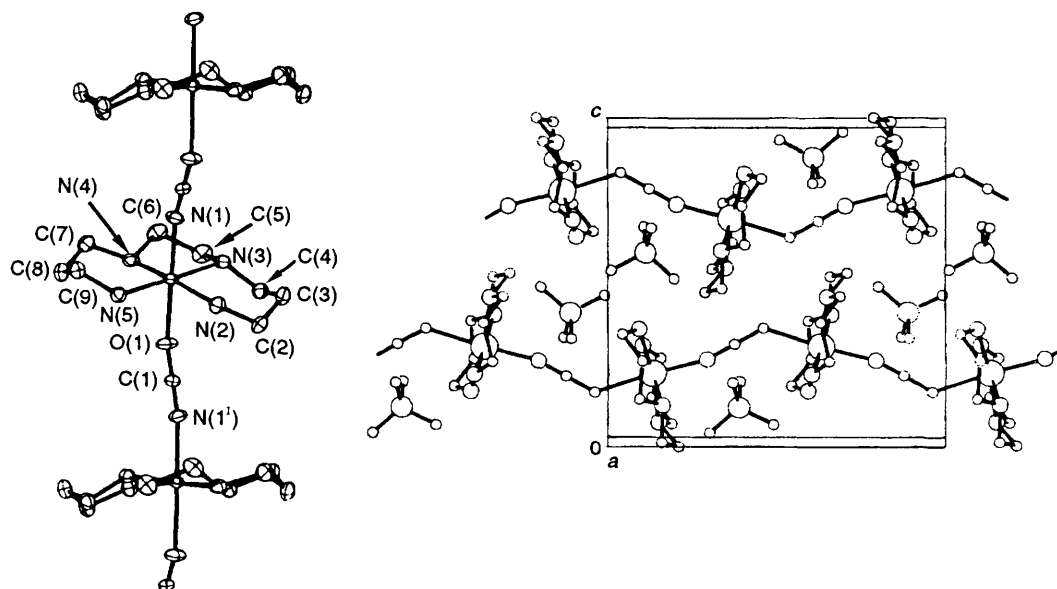
Fig. 1 Atom-labelling scheme for $[\{\text{Ni}(323\text{-tet})(\mu\text{-OCN})\}_n][\text{ClO}_4]_n$ **1** and a view of the unit cell; atom N(1') is related to N(1) by the 2_1 crystallographic axis

An atom-labelling scheme is shown in Fig. 2. Each dimeric unit consists of two $\text{Ni}(\text{Me}_6[14]\text{aneN}_4)$ fragments, in which the macrocycle is folded giving a *cis* arrangement, bridged by two end-to-end cyanate ligands. The co-ordination polyhedron around the nickel atom consists of a distorted octahedron. The Ni–N(macrocycle) distances are Ni–N(2) 2.096(3), Ni–N(3) 2.172(3), Ni–N(4) 2.110(3) and Ni–N(5) 2.193(3) Å (Table 5). Bond distances and angles involving the cyanate ligand are Ni–N(1) 2.075(3), Ni–O 2.211(3) Å, Ni–N(1)–C(17') 150.1(3),

Ni–O–C(17) 122.0(3) and O–Ni–N(1) 85.8(1)°. The two (OCN) bridges are in the same plane and the two nickel atoms are slightly out of the main $\text{Ni}_2(\text{OCN})_2$ plane in a chair arrangement (deviation of the Ni from the mean plane 0.13 Å). The torsion angle Ni–OCN–Ni is 11.6° and the dihedral angle defined by the planes $(\text{OCN})_2$ and N(1), Ni and O atoms is 4.8°. As a consequence of the lower angles in the bridging region, the Ni $\cdots$ Ni intradimer distance (5.451 Å) is lower than in compound **1**.

Table 4 Selected bond distances (Å) and angles (°) for compound **1**

O(1)–Ni	2.258(1)	N(3)–Ni	2.098(2)
N(1)–Ni	2.068(2)	N(4)–Ni	2.099(2)
N(2)–Ni	2.105(2)	N(5)–Ni	2.072(2)
C(1)–O(1)	1.220(2)	C(1)–N(1)	1.160(3)
Ni···Ni^I	6.284(1)		
O(1)–Ni–N(1)	176.9(1)	N(2)–Ni–N(3)	91.7(1)
O(1)–Ni–N(2)	90.5(1)	N(2)–Ni–N(4)	169.7(1)
O(1)–Ni–N(3)	88.4(1)	N(2)–Ni–N(5)	92.2(1)
O(1)–Ni–N(4)	80.8(1)	N(3)–Ni–N(4)	82.6(1)
O(1)–Ni–N(5)	90.1(1)	N(3)–Ni–N(5)	175.8(1)
N(1)–Ni–N(2)	92.2(1)	N(4)–Ni–N(5)	93.4(1)
N(1)–Ni–N(3)	89.9(1)	C(1^I)–N(1)–Ni	163.3(1)
N(1)–Ni–N(4)	96.4(1)	N(1^I)–C(1)–O(1)	179.6(2)
N(1)–Ni–N(5)	91.4(1)	C(1)–O(1)–Ni	132.0(1)

Table 5 Selected bond distances (Å) and angles (°) for compound **2**

O–Ni	2.211(3)	N(3)–Ni	2.172(3)
N(1)–Ni	2.075(3)	N(4)–Ni	2.110(3)
N(2)–Ni	2.096(3)	N(5)–Ni	2.193(3)
C(17)–O	1.208(4)	C(17^I)–N(1)	1.159(5)
Ni···Ni^I	5.451(1)		
O–Ni–N(1)	85.80(12)	N(2)–Ni–N(3)	84.28(12)
O–Ni–N(2)	171.54(12)	N(2)–Ni–N(4)	100.75(11)
O–Ni–N(3)	101.84(12)	N(2)–Ni–N(5)	90.16(11)
O–Ni–N(4)	85.26(10)	N(3)–Ni–N(4)	89.49(12)
O–Ni–N(5)	84.65(11)	N(3)–Ni–N(5)	169.56(11)
N(1)–Ni–N(2)	88.62(12)	N(4)–Ni–N(5)	82.85(11)
N(1)–Ni–N(3)	87.96(13)	C(17^I)–N(1)–Ni	150.1(3)
N(1)–Ni–N(4)	170.00(12)	N(1^I)–C(17)–O	177.8(4)
N(1)–Ni–N(5)	100.76(13)	C(17)–O–Ni	122.0(3)

Symmetry relation: I $-x$, $-y$, $-z$.
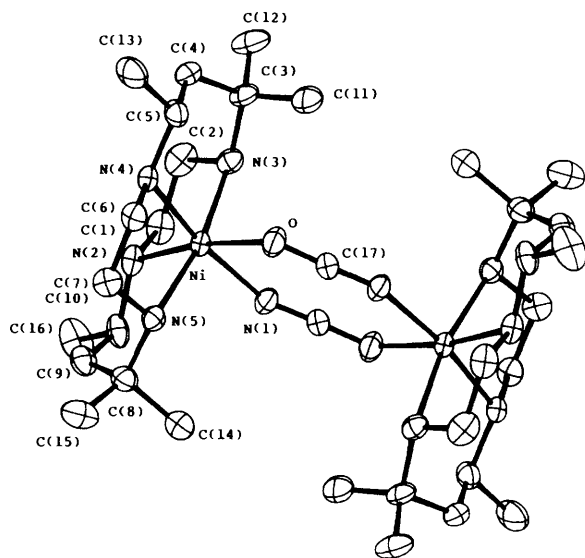
Fig. 2 Atom-labelling scheme for [{Ni(Me$_6$[14]aneN$_4$)}$_2$(μ-OCN)$_2$][ClO$_4$]$_2$ **2**

Magnetic results

Magnetic measurements for **1** (previously measured in a conventional pendulum susceptometer[18]) have been remeasured in a highly sensitive SQUID apparatus and the range of temperatures extended down to 2 K. The $\chi_M T$ product *vs.* T (per nickel atom) of [{Ni(323-tet)(μ-OCN)}$_n$][ClO$_4$]$_n$ **1** is plotted in Fig. 3(*a*). The $\chi_M T$ value of 1.24 cm^3 K mol^{-1} is practically constant in the 75–300 K range, increasing when the temperature decreases and reaching a maximum of 1.68 cm^3 K mol^{-1} at 8 K, indicating weak ferromagnetic interaction. After the maximum, the $\chi_M T$ value decreases to 1.04 cm^3 K mol^{-1} at
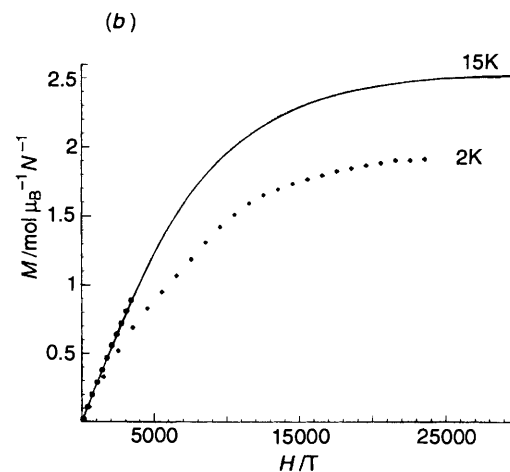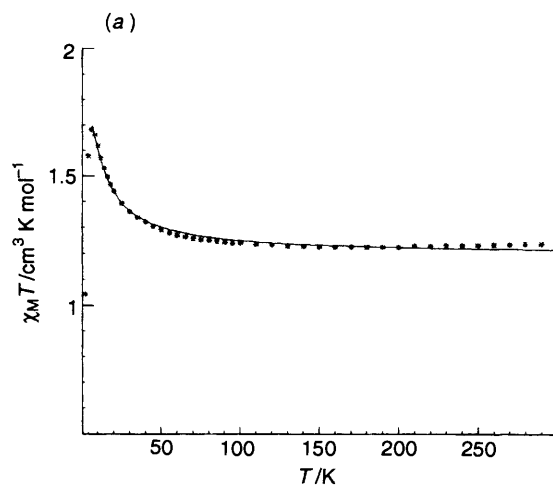
Fig. 3 (*a*) Experimental (✱✱✱) and calculated (—) plots of $\chi_M T$ (cm^3 K mol^{-1}) *vs.* T (K) and (*b*) magnetization (*M*) isotherms at 15 and 2 K up to 5 T for [{Ni(323-tet)(μ-OCN)}$_n$][ClO$_4$]$_n$ **1**. The solid line shows the fit with the Brillouin formula
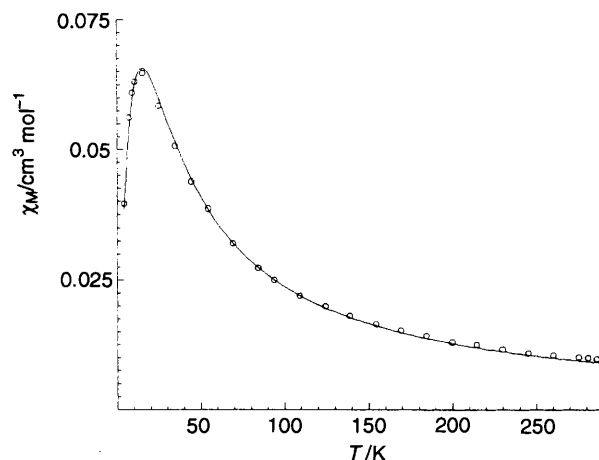
Fig. 4 Plot of χ_M (cm^3 mol^{-1}) *vs.* T (K) for [{Ni(Me$_6$[14]aneN$_4$)}$_2$-(μ-OCN)$_2$][ClO$_4$]$_2$ **2**. Solid lines indicate the best fit (see text)

2 K due to zero field splitting or weak interchain coupling. Ferromagnetic behaviour was confirmed by means of magnetization measurements at 15 and 2 K up to a maximum field of 5 T [Fig. 3(*b*)].

The plot of magnetic susceptibility per dimeric unit *vs.* T of [{Ni(Me$_6$[14]aneN$_4$)}$_2$(μ-OCN)$_2$][ClO$_4$]$_2$ **2** is shown in Fig. 4. The shape of the plot agrees with a weak antiferromagnetic [NiNi] entity: the $\chi_M T$ plot shows a 2.80 cm^3 K mol^{-1} value at

room temperature, that decreases continuously on cooling the sample and tends to zero at low temperatures. The χ_M plot shows a maximum at 15 K.

Experimental data for compound **1** have been fitted up to 8 K to the De Neef equation,[26] based upon the spin Hamiltonian $H = -2J\Sigma_{i=1}(S_iS_{i+1}) - D\Sigma_{i=1}[(S_{iz})^2 - 2/3]$, where the nickel ion is assumed to be magnetically isotropic, $\chi_M = 0.750$ $g^2/T(2 + e^{-D/kT}) + 0.375\,g^2/T[0.6666 + 2588(J/T) + 3.0675$ $(J/T)^2 - 4.7073\,(J/T)^3 - 9.1724\,(J/T)^4 + 33.135\quad(J/T)^5] +$ $1.125\,g^2/T[7.36\,(JD/T^2) + 18.53\,(J^2/DT^3) + 8.467$ $(J^3D/T^4) - 38.38\,(J^4D/T^5) + 3.81\,(J^5D/T^6) + 8.25$ $(J^2D^2/T^4) + 36.96\,(J^3D^2/T^5) + 31.13\,(J^4D^2/T^6) - 1.69$ $(JD^3/T^4) - 5.38\,(J^2D^3/T^5) + 4.946\,(J^3D^3/T^6) + 0.203$ $(JD^4/T^5) - 2.782\,(J^2D^4/T^6) + 0.4089\,(JD^5/T^6)].$

The J value was obtained by minimizing the function $R = \Sigma(\chi_M^{calc} - \chi_M^{obs})^2/\Sigma(\chi_M^{obs})^2$. The best-fit parameters obtained were $2J = +2.3$ cm^{-1}, $g = 2.19$, $D = 3.0$ cm^{-1} and $R = 8.9 \times 10^{-5}$. The intrachain J_{intra} exchange parameter was parametrized from the empirical expression[27] $kT_N = zS^2(|J_{intra} \cdot J_{inter}|)^{1/2}$, giving a value of -0.30 cm^{-1}. The best-fit parameters obtained in this work gave a similar result to the preliminary measurements,[18] improving the R factor.

Magnetization measurements were fitted to the Brillouin expression.[28] The measurement at 15 K tends to an S value of 1.15, $g = 2.22$, which confirms the ferromagnetic interactions along the chain. The measurement at 2 K shows $M/\mu_B N$ values lower than expected for $S = 1$ due to the intrachain antiferromagnetic interactions at low temperatures.

Compound **2** was fitted to the classical isotropic expression for a [NiNi] pair,[29] using the Hamiltonian $H = -JS_1S_2$, and the best-fit parameters were $J = -10.7$ cm^{-1}, $g = 2.30$ and $R = 5.1 \times 10^{-4}$. Fitting by means of the Ginsberg equation,[30] taking into account the local zero-field splitting and intradimer interactions, from the Hamiltonian $H = -JS_1S_2 - D(S_{1z}^2 + S_{2z}^2) - g\beta H(S_1 + S_2) - z'J'S\langle S\rangle$, gave a similar J value (best fit for $2J = -9.6$ cm^{-1}, $g = 2.33$, $D = -12.5$ cm^{-1} and $z'J' = 1.63$ cm^{-1} with $R = 4.8 \times 10^{-4}$).

Magneto-structural correlations for pseudohalogen bridges

The co-ordination chemistry of the cyanate ligand with nickel(II) shows a common fact: the cyanate ligand tends to co-ordinate through the nitrogen atom, giving mononuclear compounds in which the cyanate ligand acts as a terminal ligand.[31] Co-ordination compounds in which this ligand is co-ordinated only by the oxygen atom are not known. Structural confirmation of the simultaneous co-ordination by the nitrogen and oxygen atoms, in the end-to-end mode, has been reported for only one compound, [{Ni(tren)}$_2$(μ-OCN)$_2$][BPh$_4$]$_2$,[12–14] which shows a large Ni–O bond distance of 2.30 Å and a large Ni–N–C angle of 156°. The compounds reported in this work show similar characteristics in the co-ordination parameters, such as a normal Ni–N bond length, a very large Ni–O bond length (2.258 for **1** and 2.211 Å for **2**) and two strongly asymmetric bond angles, Ni–O–C in the range 122–132° and Ni–N–C greater than 150°. These bond data emphasize the gradation in the bond co-ordination angles of the pseudohalogen bridges (Table 6), which should influence the magnetic properties of the polynuclear derivatives. Analysis of Table 6 (exhaustive bond data for the bridging azido ligand can be found in refs. 4 and 10), shows that the azido ligand prefers an approximately symmetric co-ordination, whereas SCN$^-$ and SeCN$^-$ always gave a strongly asymmetric co-ordination[32–37] with characteristic values for each ligand, with typical Ni–N–C angles between 160 and 170°. Cyanato ligands give intermediate bond angles between azido and thiocyanato ligands.

The only general correlation of the magnetic behaviour with the structural parameters for the four pseudohalogen bridges N$_3^-$, OCN$^-$, SCN$^-$ and SeCN$^-$ was achieved by Duggan and Hendrickson[14] who compared the few structures reported in
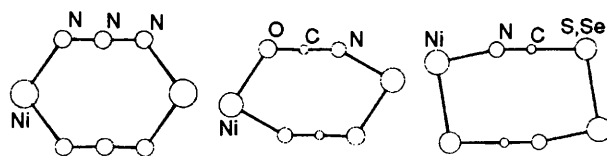
1974 for dinuclear compounds with double azido, cyanato or thiocyanato bridges. Using this very limited set of experimental data, they proposed that the main factor that influences the magnetic behaviour is the symmetry of the dimeric species, and assume that the antiferromagnetic component of J is enhanced when the two Ni–X–Y bond angles are similar, as occurs frequently for the azido bridge. On the other hand, the deviation from planarity of the bridge fragment (torsion angle Ni–XYZ–Ni) was considered less important. At present, the number of structures solved for these kind of bridges is sufficient to re-examine this proposal.

In order to approach the apparently surprising feature of two types of magnetic behaviour for the same co-ordination mode of the cyanate ligand, we have repeated the same succession of calculations that was successfully employed in the case of the azido bridge,[10] using the relationship between the square of the gaps between the xy and z^2 pairs of the molecular orbital (MO) ($\Sigma\Delta^2$) and the antiferromagnetic component of J pointed out by Hoffmann and co-workers.[38] From this model and taking into account that the pair of MOs derived from the xy atomic orbitals of the nickel atom are degenerates, $\Sigma\Delta^2$ can be defined as the square of the gap between the symmetric and antisymmetric combinations of the MOs derived from the d_{z^2} orbitals. Extended-Hückel MO calculations were performed by means of the CACAO program[39] on a dimeric fragment which can be assumed to be the translational unit of a mono-bridged infinite cyanate system (Fig. 5). As for the azido bridge, the calculations were performed by varying the Ni–O–C (β_1) and Ni–N–C (β_2) angles between 180 and 90° in steps of 5° maintaining as fixed parameter the Ni–OCN–Ni torsion angle at 180°. A second set of calculations was performed varying the Ni–OCN–Ni torsion angle for some selected values of β_1 and β_2. In all cases the remaining bond parameters were those given in Fig. 5. The results of these calculations show that the cyanate bridge acts in a very similar manner to the azido system (Fig. 6): the π non-bonding MOs of the cyanate are the most important pathway of superexchange, whereas contribution from the σ pathway to the antiferromagnetic component of J is negligible. The main difference compared with the results obtained for the azido bridge,[10] is that the magnitude of the antiferromagnetic component of J is lower than in the azido case, as a consequence of the large Ni–O distance and the asymmetry of the ligand, in good agreement with the experimental data. These results also give a similar magnitude for the antiferromagnetic component of J to those obtained by us for the thiocyanate ligand.[36] The bond angles for which the maximum antiferromagnetic coupling is expected were Ni–O–C = 120 and Ni–N–C = 105°, $\Sigma\Delta^2 = 0.08$ eV^2 (Ni–N–N = 108°, $\Sigma\Delta^2 = 0.45$ eV^2 for the azido ligand[10]). When these angles increase, the antiferromagnetic component of J decreases and takes values close to zero for a wide set of angles, as is shown in Fig. 7. The effect of the torsion angle is also similar for the azido ligand, the maximum of the antiferromagnetic component corresponding to a torsion of 180 or 0°, and a value close to zero for $J_{antiferro}$ (accidental orthogonality) for a torsion of 90°.

The behaviour of the three end-to-end cyanate compounds for which structural and magnetic data are available (Table 6) is in good accordance with the calculated properties. The two dimeric compounds [{Ni(tren)}$_2$(μ-OCN)$_2$][BPh$_4$]$_2$ and **2** show very similar bond parameters in the bridge fragment: relatively low bond angles and small torsion, and the two compounds are weakly antiferromagnetically coupled with

Table 6 Main structural and magnetic parameters for some selected nickel(II) dinuclear or one-dimensional systems with an azido bridge and all the reported complexes with a cyanato, thio- or seleno-cyanato bridge

Compound[a]	β_1[b]/°	β_2[c]/°	Γ[d]/°	$2J$/cm⁻¹	Ref.
[{Ni(en)₂}₂(μ-N₃)₂][PF₆]₂	119.3	121.1	68.5	−4.6	4
[{Ni(tn)₂}₂(μ-N₃)₂][BPh₄]₂	127.7	139.0	5.8	−114.5	4
[{Ni(333-tet)(μ-N₃)}ₙ][PF₆]ₙ	151.3	151.8	37.2	−18.5	10
[{NiL'(μ-N₃)}ₙ][ClO₄]ₙ	115.7	116.8	8.7	−97.8	11
[{Ni(tren)}₂(μ-OCN)₂][BPh₄]₂	117.1	155.0	23.7	−8.8	12–14
[{Ni(Me₆[14]aneN₄)}₂(μ-OCN)₂][BPh₄]₂	122.0	150.1	11.6	−9.6	This work
[{Ni(tren)(μ-OCN)}ₙ][ClO₄]ₙ	132.0	163.3	22.7	+2.3	This work
[{Ni(en)₂}₂I₂(μ-SCN)₂]	100.0	167.0	—	+9.0	32
[{Ni(terpy)(SCN)₂}₂(μ-SCN)₂]	100.8	159.0	63.1	+9.8	33
[{Ni₂(pn)₃(NCS)₂}(μ-SCN)₂]	100.7	165.2	42.4	+6.0	34
	105.8	142.6	63.3		
[{Ni(pn)₂}₂(μ-SCN)₂][PF₆]₂	96.2	166.7		+8.8	35
[{NiL''(SCN)(μ-SCN)}ₙ]	100.5	161.5	6.7	+2.2	36
[{Ni(en)₂(μ-SCN)}ₙ][PF₆]ₙ	100.8	171.5	—	+0.4	37
[{Ni(L'')(SeCN)₂}₂(μ-SeCN)₂]	94.7	169.2	42.2	+12.2	34

[a] en = ethane-1,2-diamine, tn = propane-1,3-diamine, 333-tet = N,N'-bis(3-aminopropyl)propane-1,3-diamine, L' = 2,3-dimethyl-1,4,8,11-tetraazacyclotetradeca-1,3-diene, pn = propane-1,2-diamine and L'' = bis(3-aminopropyl)methylamine. [b] Ni–N–N or Ni–X–C (X = O, S or Se) angle. [c] Ni–N–N or Ni–N–C angle. [d] Ni–XYZ–Ni torsion angle.
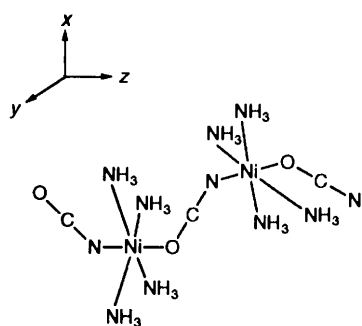

Fig. 5 Dimeric fragment; Ni–N = Ni–NH₃ = 2.10, Ni–O = 2.25, O–C = 1.21 and N–C = 1.15 Å

similar J values (−8.8 and −9.6 cm⁻¹). In contrast, compound 1 shows greater bond angles, (mainly Ni–N–C = 163.3°) and also a greater torsion angle (22.6°). As a consequence the antiferromagnetic component of J should be close to zero and the weak J_{ferro} is dominant, giving a net weak ferromagnetic character.

The analysis of all the reported structures for end-to-end pseudohalogen bridges shows that the dependence of the magnetic behaviour on these bond angles may be assumed as a general conclusion. Effectively, end-to-end azido bridges always gave antiferromagnetic coupling, showing the maximum coupling for the compound [{NiL'(μ-N₃)}ₙ][ClO₄]ₙ in which the Ni–N–N bond angles are close to 116°, Ni–N₃–Ni torsion 8.5° and $2J = -97.8$ cm⁻¹ for a single azido bridge,[11] and the minimum coupling value for [{Ni(en)₂}₂(μ-N₃)₂][PF₆]₂ (Ni–N–N 119.3 and 121.1°, torsion 8.5°, $2J = -4.6$ cm⁻¹ for a double azido bridge[4]). For the cyanate ligand, the two weak ferro- or antiferro-magnetic behaviours are possible as shown in this work, whereas the thio- and seleno-cyanate ligands, which always show Ni–X–C angles close to 100° and Ni–N–C > 160°, are always weakly ferromagnetically coupled with typical $2J$ values lower than +10 cm⁻¹.

The spin-polarization mechanism[40] for azido or cyanato ligands has been frequently invoked to explain the magnetic behaviour of the azido or cyanato polynuclear derivatives. End-on pseudohalide bridges are typically ferromagnetics, but recently[41] experimental data show antiferromagnetic coupling for copper dinuclear compounds with end-on azido bridges when the Cu–N–Cu angle is greater than 108°, and the magnitude of the antiferromagnetic coupling has been successfully correlated with this bond angle. On the other hand, our experiments show that an end-to-end cyanate bridge may
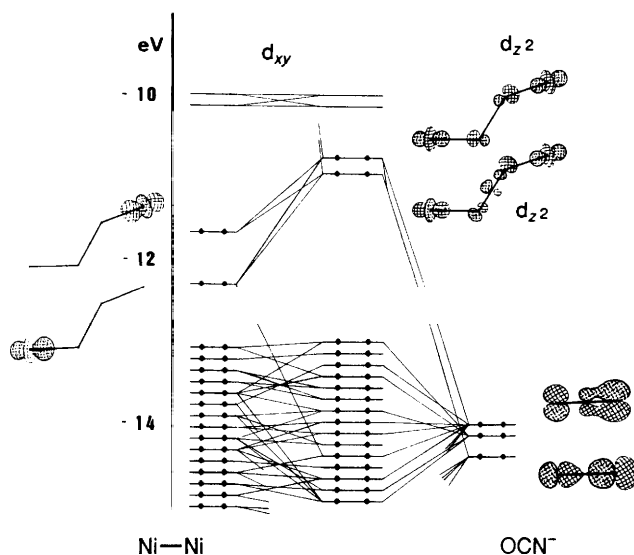

Fig. 6 MO diagram for an [(OCN)(H₃N)₄Ni–OCN–Ni(NH₃)₄-(OCN)]⁺ system calculated from the parameters Ni–N–C = 140, Ni–O–C = 120 and Ni–OCN–Ni = 0° (for remaining distances see text)

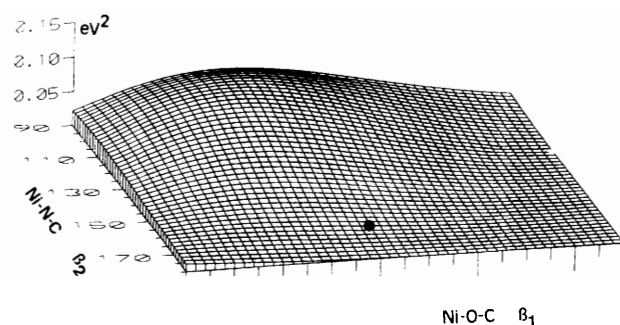Fig. 7 Plot of Δ^2 for an [(OCN)(H₃N)₄Ni–OCN–Ni(NH₃)₄(OCN)]⁺ system as a function of β_1 and β_2 maintaining the remaining parameters constant (see text). The point at $\beta_1 = 132$, $\beta_2 = 163.3°$ corresponds to Δ^2 for compound 1

allow ferromagnetic interaction to be correlated with the bond angles. On the whole, the bond-angle dependence seems a consistent model to explain the sign and magnitude when the interaction is antiferromagnetic for the pseudohalogen-bridging systems.

Conclusion

By comparison of 26 structures of the nickel–pseudohalide–nickel systems (with single or double bridges), it can be assumed that the effect of the Ni–X–Y and the Ni–XYZ–Ni torsion angles is the main factor that influences the antiferromagnetic component of the superexchange parameter J. This result, partially predicted with very limited experimental data by Duggan and Hendrickson as early as 1974, can be satisfactorily explained in terms of the relative participation of the σ and π superexchange pathways, that can give antiferromagnetic compounds through the π pathway or ferromagnetic compounds when the bond parameters allow orthogonal σ–π overlaps.

References

1 F. Wagner, M. T. Mocella, M. J. D'Aniello, A. H. J. Wang and E. K. Barefield, *J. Am. Chem. Soc.*, 1974, **96**, 2625.
2 C. G. Pierpont, D. N. Hendrickson, D. M. Duggan, F. Wagner and E. K. Barefield, *Inorg. Chem.*, 1975, **14**, 604.
3 P. Chaudhuri, M. Guttmann, D. Ventur, K. Wieghardt, B. Nuber and J. Weiss, *J. Chem. Soc., Chem. Commun.*, 1985, 1618.
4 J. Ribas, M. Monfort, C. Diaz, C. Bastos and X. Solans, *Inorg. Chem.*, 1993, **32**, 3557.
5 G. A. McLachlan, L. Spiccia, G. D. Fallon, R. L. Martin, B. Moubaraki and K. S. Murray, *Inorg. Chem.*, 1994, **33**, 4663.
6 R. Vicente, A. Escuer, J. Ribas and X. Solans, *Inorg. Chem.*, 1992, **31**, 1726.
7 A. Escuer, R. Vicente, J. Ribas, M. S. El Fallah and X. Solans, *Inorg. Chem.*, 1993, **32**, 1033.
8 A. Escuer, R. Vicente, J. Ribas, M. S. El Fallah, X. Solans and M. Font-Bardia, *Inorg. Chem.*, 1993, **32**, 3727.
9 A. Escuer, R. Vicente, J. Ribas, M. S. El Fallah, X. Solans and M. Font-Bardia, *J. Chem. Soc., Dalton Trans.*, 1993, 2975.
10 A. Escuer, R. Vicente, J. Ribas, M. S. El Fallah and X. Solans, *Inorg. Chem.*, 1994, **33**, 1842.
11 R. Vicente, A. Escuer, J. Ribas, M. S. El Fallah, X. Solans and M. Font-Bardia, *Inorg. Chem.*, 1995, **34**, 1278.
12 D. M. Duggan and D. N. Hendrickson, *J. Chem. Soc., Chem. Commun.*, 1973, 411.
13 D. M. Duggan and D. N. Hendrickson, *Inorg. Chem.*, 1974, **13**, 2056.
14 D. M. Duggan and D. N. Hendrickson, *Inorg. Chem.*, 1974, **13**, 2929.
15 R. Cortés, M. I. Arriortua, T. Rojo, D. Beltran and T. Debaerdemaeker, *Transition Met. Chem.*, 1986, **11**, 238.
16 M. I. Arriortua, R. Cortés, J. L. Mesa, L. Lezama, T. Rojo and G. Villeneuve, *Transition Met. Chem.*, 1988, **13**, 371.
17 A. Escuer and R. Vicente, unpublished work.
18 A. Escuer, R. Vicente, J. Ribas, M. S. El Fallah, X. Solans and M. Font-Bardia, *Inorg. Chim. Acta*, 1994, **216**, 5.
19 F. Valach and M. Dunaj-Jurco, *Acta Crystallogr., Sect. B*, 1982, **38**, 2145.
20 R. Vicente, A. Escuer, E. Peñalva, X. Solans and M. Font-Bardia, *J. Chem. Soc., Dalton Trans.*, 1994, 3005.
21 A. M. Tait and D. H. Busch, *Inorg. Synth.*, 1976, **18**, 4.
22 G. M. Sheldrick, *Acta Crystallogr., Sect. A*, 1990, **46**, 467.
23 G. M. Sheldrick, SHELX 76, program for crystal structure determination, University of Cambridge, 1976.
24 G. M. Sheldrick, SHELXL 93, University of Göttingen, 1993.
25 *International Tables for X-Ray Crystallography*, Kynoch Press, Birmingham, 1974, vol. 4, pp. 99–110, 149.
26 T. De Neef, Ph.D. Thesis, Eindhoven, Netherlands, 1975.
27 P. M. Richards, *Phys. Rev. B*, 1974, **10**, 4687.
28 P. L. Carlin, *Magnetochemistry*, Spring-Verlag, Berlin, 1986.
29 C. J. O'Connor, *Prog. Inorg. Chem.*, 1982, **29**, 239.
30 A. P. Ginsberg, R. C. Sherwood, R. W. Brookes and R. L. Martin, *J. Am. Chem. Soc.*, 1971, **393**, 5927.
31 *Comprehensive Coordination Chemistry*, ed. G. Wilkinson, R. D. Gillard and J. A. McCleverty, Pergamon, Oxford, 1987, vol. V.
32 A. P. Ginsberg, R. L. Martin, R. W. Brookes and R. C. Sherwood, *Inorg. Chem.*, 1972, **11**, 2884.
33 T. Rojo, R. Cortés, L. Lezama, M. I. Arriortua, K. Urtiaga and G. Villeneuve, *J. Chem. Soc., Dalton Trans.*, 1991, 1779.
34 R. Vicente, A. Escuer, J. Ribas, X. Solans and M. Font-Bardia, *Inorg. Chem.*, 1993, **32**, 6117.
35 M. Monfort, J. Ribas and X. Solans, *Inorg. Chem.*, 1994, **33**, 4271.
36 R. Vicente, A. Escuer, J. Ribas and X. Solans, *J. Chem. Soc., Dalton Trans.*, 1994, 259.
37 M. Monfort, C. Bastos, C. Diaz, J. Ribas and X. Solans, *Inorg. Chim. Acta*, 1994, **218**, 185.
38 J. P. Hay, J. C. Thibeault and R. Hoffmann, *J. Am. Chem. Soc.*, 1975, **97**, 4884.
39 C. Mealli and D. M. Proserpio, *J. Chem. Educ.*, 1990, **67**, 3399.
40 M. F. Charlot, O. Kahn, M. Chaillet and C. J. Larrieu, *J. Am. Chem. Soc.*, 1986, **108**, 2574.
41 L. K. Thompson, S. S. Tandon and M. E. Manuel, *Inorg. Chem.*, 1995, **34**, 2356.